Vibrational spectroscopic analysis of hydroxyapatite in HYP mice and individuals with X-linked hypophosphatemia

Eva Amenta, Helen E. King, Holger Petermann, Vuk Uskoković, Steven M. Tommasini and Carolyn M. Macica

Abstract

Background: X-linked hypophosphatemia (XLH) is the most common form of familial phosphate-wasting disorders, due to an inactivating mutation in the phosphate-regulating neutral endopeptidase, X-linked gene. Persistent osteomalacia, enthesophytes, osteophytes, degenerative arthritis and dental abscesses/periodontal disease dominate the adult disorder. However, the impact of insufficient phosphate on hydroxyapatite composition, the major inorganic component of bone and teeth, is unknown in individuals with XLH.

Methods: Using Raman spectroscopy, the carbonate (CO_3^{2-}) to phosphate (PO_4^{3-}) ion ratio was measured in HYP and wild-type mice and in primary and permanent teeth from XLH individuals and unaffected controls.

Results: There was a significant difference in carbonate ion substitution between the HYP and wild-type femoral cortical bone (0.36 ± 0.08 *versus* 0.24 ± 0.04; $p < 0.001$). Carbonate ion substitution levels were also higher in permanent XLH teeth compared with unaffected individuals (0.39 ± 0.12 *versus* 0.23 ± 0.04; $p < 0.001$), but not in primary teeth (0.29 ± 0.11 *versus* 0.26 ± 0.02; $p = 0.29$). Complementary Fourier transform infrared analyses demonstrated higher relative intensities of the four major vibrational bands originating from the carbonate anion in XLH teeth compared with unaffected controls.

Conclusion: Ionic substitution within the crystal lattice is a common feature of hydroxyapatite and one that confers the physiological properties of bone that impact mechanical strength and the process of bone remodeling. Our data demonstrating anionic substitution in human dentin from individuals with XLH validate the use of dentin as a proxy for bone and to better understand the molecular adaptations that occur in the biochemical milieu of XLH.

Keywords: carbonate, cortical bone, dentin, hydroxyapatite composition, phosphate, XLH

Received: 6 March 2018; revised manuscript accepted: 20 July 2018.

Correspondence to:
Carolyn M. Macica
Frank H. Netter MD School of Medicine, Quinnipiac University, 275 Mt. Carmel Avenue, NH-MED MNH-311H, Hamden, CT 06518, USA
carolyn.macica@quinnipiac.edu

Eva Amenta
Department of Medical Sciences, Frank H. Netter, M.D., School of Medicine at Quinnipiac University, North Haven, CT, USA

Helen E. King
Department of Earth Sciences, Utrecht University, Utrecht, The Netherlands

Holger Petermann
Department of Geology and Geophysics, Yale University, New Haven, CT, USA

Vuk Uskoković
Department of Biomedical and Pharmaceutical Sciences, School of Pharmacy, Chapman University, Irvine, CA, USA

Steven M. Tommasini
Department of Orthopaedics and Rehabilitation, Yale University, New Haven, CT, USA

Introduction

X-linked hypophosphatemia (XLH) is a familial phosphate-wasting disorder characterized by childhood rickets and osteomalacia, with osteomalacia persisting throughout adulthood.[1] XLH arises as a consequence of an inactivating mutation of the PHEX (phosphate-regulating endopeptidase homolog, X-linked) gene which, for reasons that are still not entirely understood, results in elevated levels of the circulating hormone, fibroblast growth factor-23 (FGF23). FGF23 is a phosphatonin that regulates renal phosphate handling, mediating the excretion of phosphate in the maintenance of normal serum phosphate levels.[2,3] In addition, FGF23 also negatively regulates 1,25-dihydroxyvitamin D biosynthesis by inhibiting 1a hydroxylase (CYP27B1) and promotes its catabolism by activation of 24 hydroxylase (CYP24A1).[4] Elevated levels of FGF-23 create inappropriate phosphaturia leading to physiologically low levels of circulating phosphate. Loss of phosphate has been associated with multiple impairments including
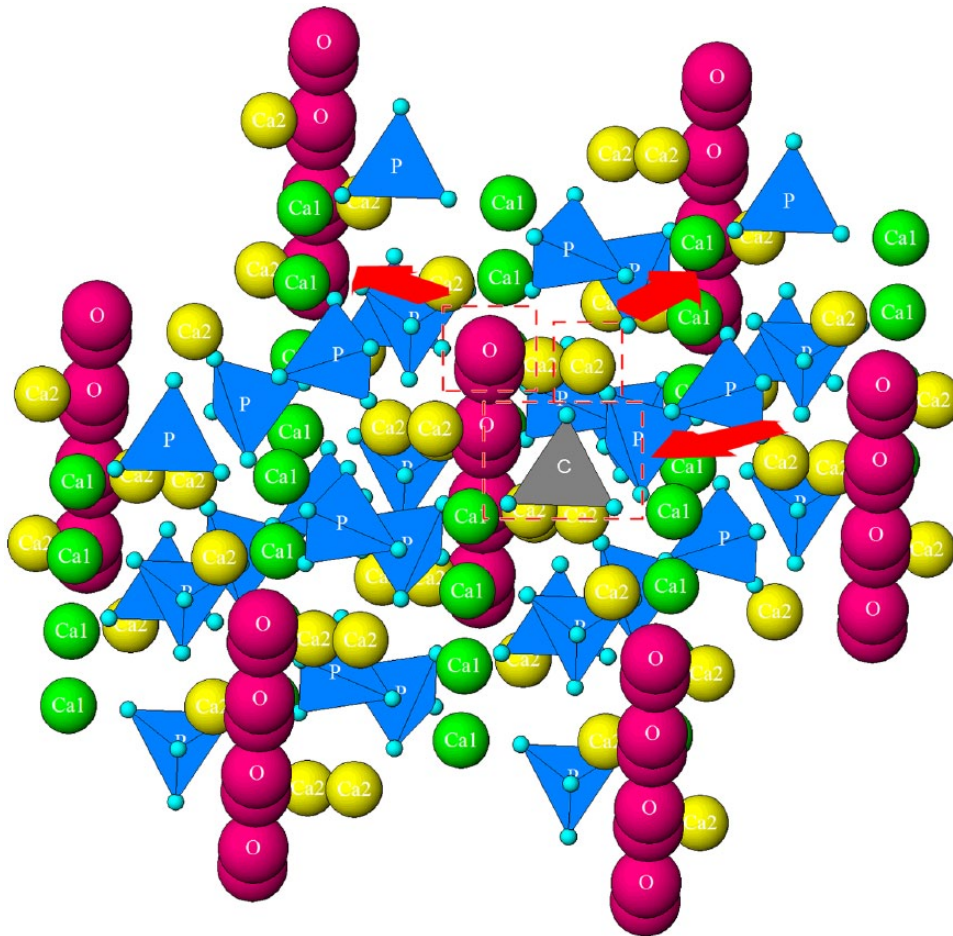
Figure 1. Crystal structure of hydroxyapatite showing a single phosphate-to-carbonate substitution. Substitution is shown in the center, along with two typical vacancies forming to balance the resulting cationic charge excess: Ca^{2+} and OH^-. Different ionic elements are represented with different colors: columnar, Ca1 calcium in green, hexagonal, Ca2 calcium in yellow, hydroxyl in magenta, phosphate in blue, and carbonate in gray. Red arrows indicate that these ions will be removed, and vacancies formed with carbonate substitution.

tibial bowing, abnormal gait, bone pain, tinnitus and vertigo and impaired growth secondary to a rachitic growth plate.[5] In addition to persistent osteomalacia, other comorbidities of XLH include enthesophytes, osteophytes, degenerative arthritis, and dental abscesses, decay, and periodontal disease.[6–8]

The mineral composition of bone is a form of hydroxyapatite, an inorganic calcium phosphate mineral with the stoichiometric unit cell formula $Ca_{10}(PO_4)_6(OH)_2$. Apatite is considered the mineral reservoir of the body and it is estimated that more than half of all the elements of the Periodic Table can be stably incorporated in it.[9] These regularly occurring ionic substitutions have critical effects on mineral properties such as mechanical strength, brittleness, crystallinity,

and solubility.[10] In biological tissues, such as bone and dentin, the most abundant substitution is carbonate (CO_3^{2-}), with normal bone containing 2–8 wt%.[11] Carbonate can be accommodated at two sites in the crystal structure: A-type replaces the hydroxyl group (OH^-) and B-type the phosphate group (PO_4^{3-}). Even though high temperatures are required for A-type substitution in synthetic apatites, bone and dentin are mixtures of A and B-types.[12] Carbonate in the apatite structure is responsible for a decrease in the degree of crystallinity, weakening the bonds and increasing the mineral solubility.[9,11,13] The crystal structure of hydroxyapatite with a single phosphate-to-carbonate substitution (along with two typical vacancies that form to balance the resulting cationic charge excess – Ca^{2+} and OH^-) is shown in Figure 1.

The dentin matrix of teeth is analogous to the extracellular matrix of bone including the inorganic hydroxyapatite composition and organic extracellular matrix proteins.[14] Tooth development involves formation of both primary and permanent teeth. Primary teeth develop in a two-fold manner. The tooth crown is developed *in utero* and the root develops after birth. The permanent tooth structure begins initial calcification at 3 months postnatal with crown development occurring between ages 4 and 8 years. Odontogenesis and osteogenesis follow a similar process of mineralization with defects in mineralization not only affecting the integrity of bone, but teeth as well.[15] However, the impact of insufficient phosphate on hydroxyapatite composition, the major inorganic component of bone and teeth, is unknown in individuals with XLH.

Previously, we have shown that the ratio of phosphate-to-carbonate ion substitution in cortical bone mineral matrix is potentiated in HYP mice, a murine model of XLH.[16] However, a major obstacle to the study of human apatite in XLH is the need for tissue. Here, using tooth dentin as a proxy for bone, we test the hypothesis that this phenomenon is reproduced in individuals with XLH as a consequence of phosphate-wasting.

Materials and methods

Tooth sample collection

Human teeth were collected to measure carbonate ion substitution in hydroxyapatite from individuals with XLH or unaffected controls. This study was granted exemption from review by the institutional review board at Yale University School of Medicine (HIC protocol #1403013639) in accordance with federal regulation 45 CFR 46.101(b)(4), which covers research involving the collection or study of existing data, documents, records, pathological specimens, or diagnostic specimens, if these sources are publicly available or if the information is recorded by the investigator in such a manner that participants cannot be identified, directly or through identifiers linked to the participants. No identifiers were collected for this study and coding was used to link the anonymous samples to the anonymous data. Inclusion criteria for submitting teeth was a confirmed diagnosis of XLH either based on the clinical validation (physical exam, blood chemistries, diagnostic imaging and family history) or

by genetic testing of the PHEX gene. All children in this study (7/7) had confirmed genetic testing of the PHEX gene while adult participants were diagnosed either by clinical validation (6/9) or genetic testing. In contrast to primary maxillary and mandibular tooth calcification in humans, which begins within a range of 14–19 weeks *in utero*, permanent teeth undergo mineralization entirely during the postnatal period[17] during which hypophosphatemia persists despite therapy. All study participants with XLH were treated during childhood and treated until growth plate closure. Adult management, for which there is no current consensus, was initiated in all patients only during symptomatic periods of pain related to osteomalacia and microfracture. Therapeutic goals in both populations are not to restore serum phosphate levels to a normal range, because of the significant risk of soft tissue calcification.[5,18]

Primary teeth (male and female) were obtained and all were a consequence of normal deciduous tooth loss. Adult teeth (male and female) were collected as a consequence of tooth extraction. There was little variability in carbonate ion substitution between sexes in our relatively small sample size for each group (control and XLH) so data were combined. Primary teeth were collected from seven different individuals diagnosed with XLH ($n = 7$, 8.9 ± 1.7 years) and individuals from the unaffected control population ($n = 5$, 8.4 ± 1.1 years). Extracted permanent teeth (molars and canines) were collected from individuals diagnosed with XLH ($n = 9$, 46.9 ± 8.6 years) and individuals from the unaffected control population ($n = 5$, 53.5 ± 10.2 years). Teeth were embedded in methyl methacrylate, cut longitudinally, and crown dentin analyzed by Raman spectroscopy, as described.

HYP and wild-type littermate mice

Mice were fed standard chow *ad libitum* and tap water. All mice ($n = 4$/group) were maintained in accordance with the recommendations in the Guide for the Care and Use of Laboratory Animals and procedural protocol was approved by Yale's Institutional Animal Care and Use Committee. Female mice were sacrificed at 5 months of age, the femora were harvested, cleaned of soft tissue, embedded in (poly)methyl methacrylate (PMMA), cut longitudinally, and mid-diaphysis cortical bone was analyzed by Raman spectroscopy as described below.

Matrix chemical composition determined by Raman spectroscopy

Mineral substitutions into the hydroxyapatite lattice are important to crystal size, density, and solubility and abnormal bone mechanical properties have been correlated with abnormal carbonate content, an anionic substituent of phosphate, in bone and in metabolic bone disorders.[19–24] Raman spectroscopy was performed, as previously described.[16] Briefly, a Horiba HR800 Raman microspectrometer equipped with an Olympus BX-41 light microscope and 100 × objective was used to examine spatially resolved, distinct areas of teeth in order to determine the compositional variations of the mineral within single tooth and between teeth of individuals with XLH and controls. A 532 nm Nd-YAG laser was used for the analysis (30 s integrated 10 times), however, the bone and dentin samples are sensitive to the laser at this wavelength, therefore a 0.6 optical density filter was placed into the laser light path before passing through a 300 μm confocal hole to lower the laser power impacting the sample. The surface of the sample cross section was imaged using the incorporated optical microscope before and after the measurement to ensure that no laser-induced burns occurred on the sample surface during the spectrum acquisition. After the light was backscattered from the sample it passed through a 200 μm slit before being dispersed on a 1800 grooves/mm grating and analyzed using a charge coupled device detector. All spectra were collected at room temperature. Between one and four maps per tooth of the dentin in the crown of the tooth were taken using a 4 × 4 grid of 16 points. The spot size of the laser beam with the 100× objective lens was ~1 μm, therefore a step size of 3 μm was used between each spot analysis in the map grids. The total size of each map was 13 μm ×13 μm. To minimize the time associated with the laser exposure of the bone tissue, each spectrum in the mapped sites was acquired only in the spectral region of interest between 800 and 1200 cm^{-1}. The bands in the corrected bone spectra were subsequently fit using eight peaks: 925, 948, 960, 1003, 1025, 1045, 1070 and 1100 cm^{-1}, to evaluate the contribution of the carbonate and phosphate from the bone samples, as described previously by Awonusi and colleagues.[25] Dentin was discriminated from enamel based on the absence of a band at 1003 cm^{-1} in enamel corresponding to the most intense collagen peak in our spectral region of interest.[25–27] Data were collected and analyzed using Labspec 5 software (Edison, NJ, USA). Synthetic standards of B-site-substituted carbonated hydroxyapatite provided and previously analyzed by Prof. Yoder, Franklin and Marshall College, USA,[19] were also analyzed for comparison. The background was removed followed by de-spiking (removal of artifacts) and smoothing (for better visibility of individual peaks). Spectra with fluorescent background were removed using a linear fit of the spectral region of interest, spectra with high fluorescent background were not used for further data analyses. Overall, eight peaks were fitted at the positions mentioned previously. The eight peaks were then fixed in those positions where a fitting algorithm was applied that combines Gaussian and Laurencin bell curves with 1,000,000 repetitions. Fitting was repeated until the error (a least-squares sum) was minimized.

Fourier transform infrared (FTIR) analysis

FTIR analysis was performed on powdered dentin obtained from the primary teeth of individuals with XLH and healthy controls. The powdering process involved manually scraping the material off the dentin slices or whole teeth with a razor blade. Analysis was done on a Bruker Alpha Platinum attenuated total reflection (ATR) spectrometer with a single-reflection diamond/WC composite ATR module, in the 4000–400 cm^{-1} wavenumber range and with the spectral resolution of 2 cm^{-1}. Integrated intensities of the bands were measured by calculating a background function and deconvoluted peak profile using an automated Gaussian-fitting routine (OriginPro 2018, Northampton, MA, USA). The integration time was circa 1 s and no smoothing functions were applied prior to integration. Acquisition of spectra was repeated with duplicate samples to ensure reproducible results.

Statistical analysis

All statistical analyses were performed using SPSS software (IBM, New York, NY, USA) and data are presented as mean ± standard error, with significance indicated at $p \leqslant 0.05$.

Murine bone samples. Statistical significance between HYP and wild-type was determined using a Student's *t*-test.

Tooth sample analysis. To compare the carbonate-to-phosphate ratio of teeth between XLH and controls, a linear mixed model with a fixed effect for group and a random subject intercept was
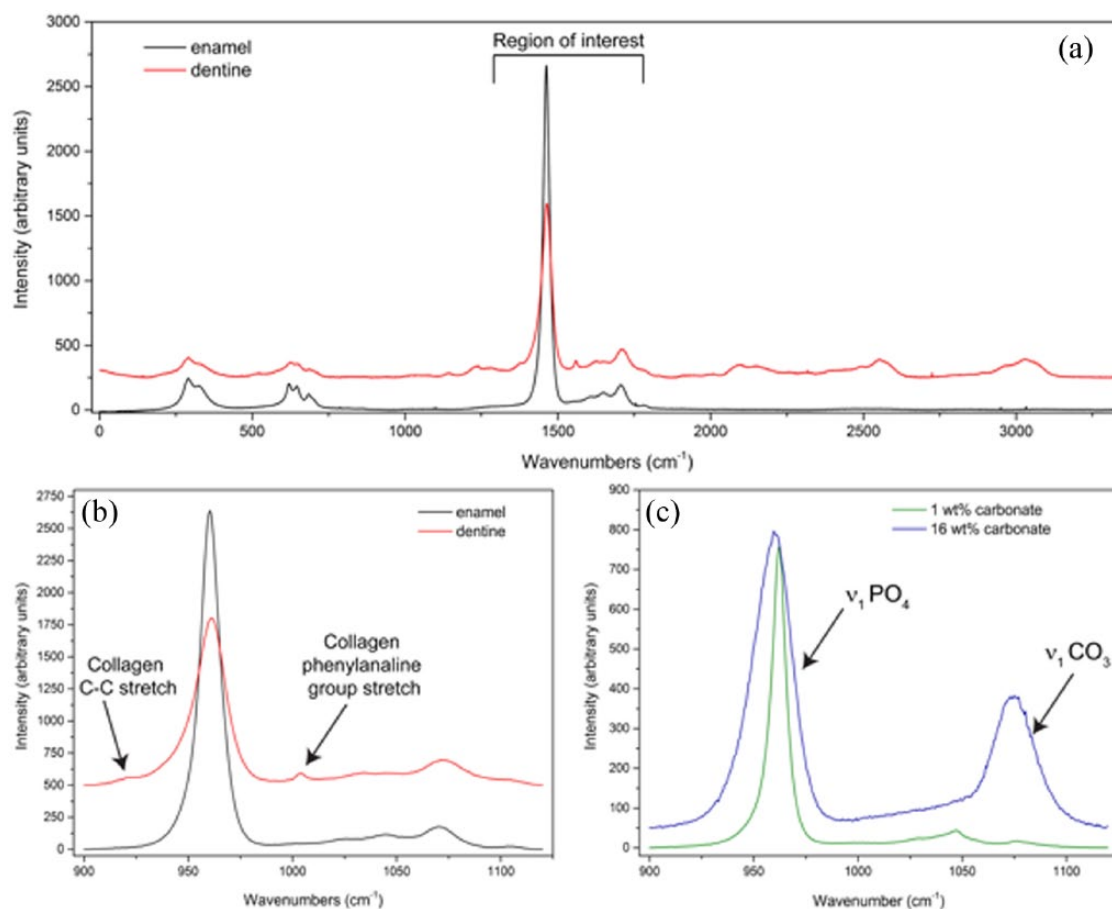
Figure 2. Raman spectroscopy individual spectra. (a) Spectral peaks at 925, 948, 960, 1003, 1025, 1045, 1070 and 1100 cm^{-1}. (b) Enamel spectrum superimposed on a dentin spectrum showing the absence of collagen peaks (collagen C-C bond stretch at 925 cm^{-1} and collagen phenylalanine stretch at 1003 cm^{-1}). (c) Known carbonate standards with differing amounts of carbonate represented at peak 1070 cm^{-1}.

used. To assess how much of the overall variability in the carbonate-to-phosphate ratio was attributed to varying readings of the same tooth (within-subject), as opposed to measurements between teeth from different patients (between-subject), a linear mixed model was used to estimate the proportion of total variance that was attributed to the within-subject variability.

Results

As can be observed in Figure 2(a), dentin and enamel produce distinctly different Raman spectra due to the presence of the organic collagenous matrix in dentine, similar to that observed in bone.[15,28] The vibrational modes associated with the organic matrix result in multiple additional bands in the spectral region between 2000 and 3500 cm^{-1} and as shown in Figure 2(b), bands close to 800 cm^{-1} and a distinct band at

1003 cm^{-1}.[29] As the collagen band at 1003 cm^{-1} is within our spectral region of interest, this band was used to differentiate between enamel and dentine sampling areas in the Raman spectra. The most prominent bands observed in the spectrum of hydroxyapatite were different modes of the symmetric, nondegenerated P-O stretch of the PO_4^{3-} ion tetrahedron, $\nu1$, spectra at 948 and 960 cm^{-1}. Incorporation of carbonate into the mineral hydroxyapatite structure of synthetic carbonated hydroxyapatites [Figure 2(c)] results in an increase in the 1070 cm^{-1} band intensity, which is associated with the ν_1 symmetrical carbonate stretching mode.[30] Thus, the ratio of carbonate ν_1 to phosphate ν_1 band areas in abiotic standards were used to compare with the ratio calculated from our biological samples, as described by Awonusi and Penel.[25,30] This also allows us to compare between different samples as absolute values cannot be compared across
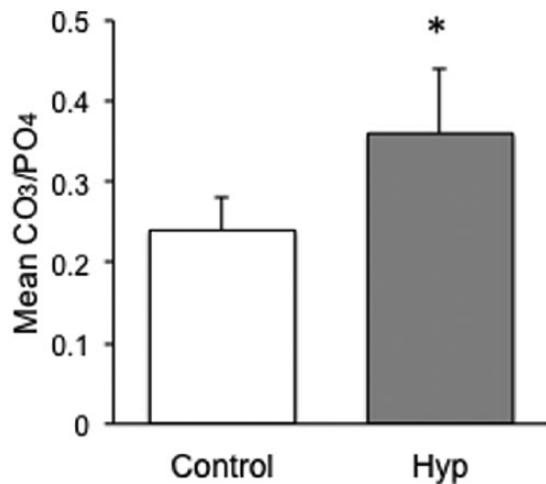
Figure 3. CO_3/PO_4 ratio analysis in wild-type *versus* HYP cortical bone. HYP mice femur displayed a greater carbonate ion substitution compared with wild-type ($p < 0.001$; $n = 4$/group). Error bars represent the standard error.
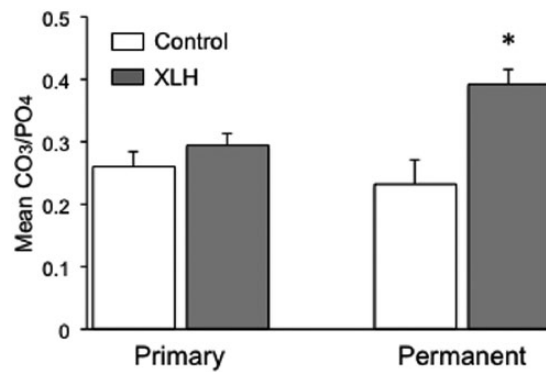

Figure 4. Comparison of CO_3 matrix incorporation in primary and permanent teeth in individuals with XLH compared with controls. Raman spectroscopy analysis demonstrated no statistically significant difference between the primary teeth of individuals with XLH ($n = 7$) compared with controls ($n = 5$), but a significant difference (*) between permanent teeth of individuals with XLH ($n = 9$) compared with controls ($n = 5$; $p < 0.001$). Error bars represent standard error.
XLH, X-linked hypophosphatemia.

samples because the intensity of spectra is dependent on the laser intensity, amount of material analyzed within the laser spot, and the Raman scattering efficiencies of the molecular groups. Carbonate-phosphate ratios observed in HYP and wild-type femurs (Figure 3) show that relative to control mice, HYP mice had a significant increase in carbonate ion substitution in cortical bone (0.36 ± 0.08 *versus* 0.24 ± 0.04; $p < 0.001$).

To determine whether carbonate ion substitution similarly occurred in mineral samples obtained from individuals with XLH, Raman analysis was performed on human tooth dentin. Despite the physiologic differences in turnover between bone and tooth dentin, the composition of dentin hydroxyapatite, within a type-1 collagen matrix, serves as an ideal proxy for studying mineralization in human subjects due to the lack of availability of XLH patient bone samples.[14,31] We compared both primary and adult permanent teeth between control and affected populations (Figure 4). Odontogenic mineralization of primary teeth occurs during a fixed period of time *in utero*, yielding insight into whether the aberrant maternal mineral status of XLH impacts mineralization of the developing fetus. Analysis of primary teeth revealed no statistically significant difference between individuals with XLH compared with unaffected controls (0.29 ± 0.11

versus 0.26 ± 0.02; $p = 0.29$). In contrast, comparison of permanent teeth in patients with XLH, compared with unaffected controls, revealed a statistically significant increase in the amount of hydroxyapatite carbonate ion substitution (0.39 ± 0.12 *versus* 0.23 ± 0.04; $p < 0.001$). The variability of carbonate ion substitution was also assessed within each XLH permanent tooth sample and compared with the variability of carbonate ion substitution between individual patient tooth samples. Variability within each tooth sample was equivalent to variability between patients (variances: 0.0099 ± 0.0010 *versus* 0.0093 ± 0.0040, respectively), suggesting that variation in levels of carbonate substitution is intrinsic to the disease and not primarily a function of the differences that exist between individual environmental factors.

The complementary qualitative FTIR analysis demonstrated a more pronounced upshift shoulder of the triply degenerated asymmetric stretching mode of the P-O bond, v_3, in the XLH dentin samples compared with the healthy control [Figure 5(a)]. The intensification of this shoulder in the 1070–1090 cm^{-1} region, which is due to the symmetric stretch of the carbonate ion, v_1, confirms the greater degree of phosphate-to-carbonate substitutions in the XLH individuals compared with the wild-type controls. Given that the maximum of this band was detected closer to
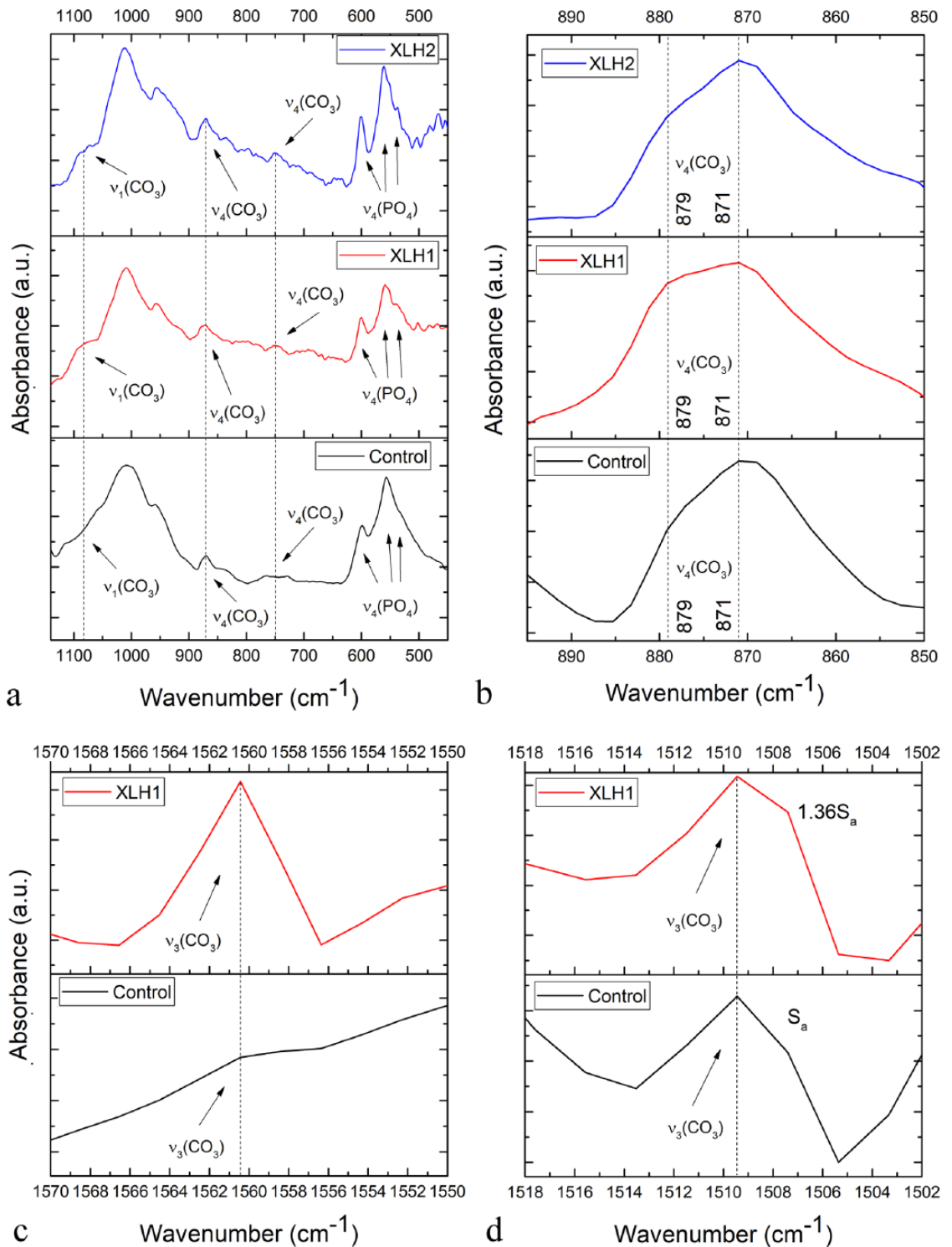
Figure 5. FTIR spectra of the permanent tooth dentins derived from individuals with XLH and the healthy control in: (a) the 1150–450 cm⁻¹ region, showing the most prominent phosphate and carbonate bands in the dentin spectrum; (b) 900–850 cm⁻¹ region, showing the $v_4(CO_3)$ band and distinguishing between A-type (879 cm⁻¹) and B-type (871 cm⁻¹) carbonate substitutions; (c) 1570–1550 cm⁻¹ region, showing one far blue end component of the $v_3(CO_3)$ multiplet; and (d) 1508–1502 cm⁻¹ region, showing another far blue end component of the $v_3(CO_3)$ multiplet. S_a denotes the integrated intensity of the $v_3(CO_3)$ band.
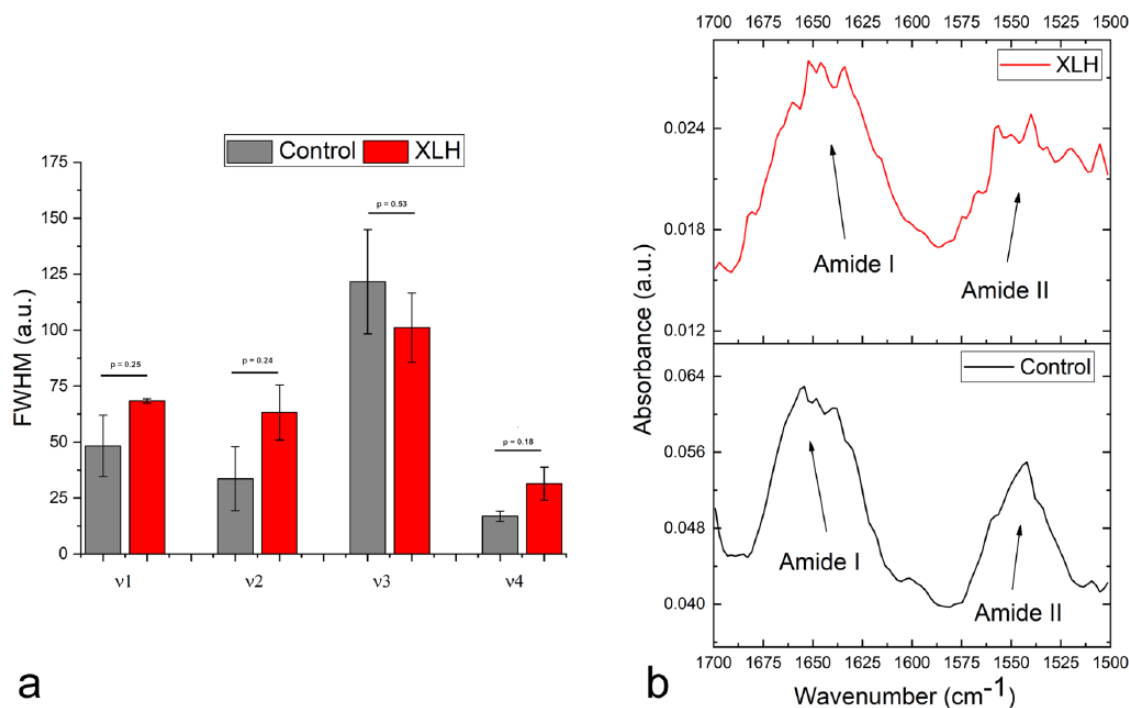FTIR, Fourier transform infrared; XLH, X-linked hypophosphatemia.

Figure 6. (a) Full-widths at half-maximum (FWHM) values for the four major phosphate vibrations, $\nu_1 - \nu_4$, in the spectrum of the dentin of individuals with XLH compared with the healthy controls. Error bars represent standard error of the mean. (b) Intensity ratio between amide I and amide II bands originating predominantly from the carbonyl stretching vibration in peptide bond groups and the coupled N-H bend and C-N stretch.

1080 cm^{-1} than to 1110 cm^{-1}, it indicates that the carbonated apatite in both types of samples is, expectedly, B-type, where carbonate ions substitute phosphates and not channel hydroxyls.[12] In addition, this carbonate band becomes broader in XLH, suggesting a lesser degree of order in the carbonate ion environment, being consequential to higher degrees of substitution and lattice strain. The splitting of the triply degenerated bending mode, ν_4, of the O-P-O bond, with the theoretical maxima at 601, 575 and 561 cm^{-1}, is further indicative of a change in the long-range ordering of the phosphate anion in the XLH dentin accompanying the carbonation of the structure [Figure 5(a)]. The same effect can be observed from the higher intensity ratio between 880 and 872 cm^{-1} bands of the $\nu_2(CO_3)$ doublet in the XLH samples [Figure 5(b)], indicating a greater, albeit finite degree of substitution of OH^- (A-type) lattice sites by the carbonates in apatite.[12] Namely, increased carbonate presence induces lattice distortion, enabling the carbonates to begin to partially occupy the hydroxyl channel sites, an effect that is minimally present at low carbonate contents and in the absence of the thermal treatment.

Similar intensifications of carbonate bands in the XLH dentin were detected for the $\nu_4(CO_3)$ mode peaking at 755 cm^{-1} and to some extent for $\nu_2(CO_3)$ mode peaking at 872 cm^{-1} [Figure 5(a)] as well as for the $\nu_3(CO_3)$ quadruplet in the 1418–1560 cm^{-1} region, including most prominently the far blue end maxima at 1560 cm^{-1} [Figure 5(c)] and 1509 cm^{-1} [Figure 5(d)].

Full-widths at half-maximum (FWHM) of solid state vibration modes in apatites is widely accepted to be inversely proportional to crystallinity and although the effect is most easily observed on the most intense, 960 cm^{-1} ν_1 symmetric stretching mode of the phosphate ion,[22] the other three major phosphate bands, ν_2, ν_3 and ν_4, can be used for the same correlation.[32,33] The analysis of the vibration band halfwidths showed the broadening of three of the four major phosphate bands in XLH dentin (ν_1, ν_2 and ν_4), indicating lesser crystalline symmetry resulting directly from the lattice disordering due to carbonate substitutions and the formation of paired $Ca^{2+}-OH^-$ vacancies accompanying these substitutions [Figure 6(a)]. However, the analysis of the ratio of absorptions at 1020 and 1030 cm^{-1},

directly proportional to the crystallinity index of the material,[34] did not result in a difference between the XLH sample and the control (1.081 ± 0.124 *versus* 1.078 ± 0.004, respectively). In turn, the observed splitting of the bending mode of the phosphate anion in the 500–620 cm⁻¹ range into more distinct transverse and longitudinal components suggested an even higher crystallinity of the XLH sample.[35] This effect cannot be explained as the result of the sole effect of carbonate-to-phosphate substitution on the crystalline order, but may be biological in origin, presumably involving a reduction in the amount of amorphous apatite in the XLH dentin. Amorphous apatite is known to be a precursor for the mineralization of apatite[36] and its amount drops with age,[37] entailing the reduction in the remodeling and remineralization capacity of the tissue. One such intrinsic induration of the mineral can be responsible for causing some of the pathological conditions associated with the XLH. To check for the possible contributions from the underlying bone matrix bands, the intensity ratio between amide I and amide II bands in XLH samples and controls and their halfwidths were analyzed. Although the intensity ratio between amide I and amide II bands originating predominantly from the carbonyl stretching vibration in peptide bond groups and the coupled N-H bend and C-N stretch, respectively, was the same for both the XLH dentin and the control, both bands adopt a ruffled profile in the XLH samples [Figure 6(b)]. The bands split into a fine structure and broaden in the process, suggesting the possibility that there is some level of structural distortion of the organic matrix in the XLH samples accompanying the aforementioned mineral effect.

Discussion

Using a murine model of XLH, we have found that cortical bone apatite analyzed by Raman spectroscopy in HYP mice has a significant increase in carbonate ion substitution compared with wild-type mice (Figure 3). In addition, our previous studies using FTIR analysis showed that collagen crosslinking, mediated by lysine and hydroxylysine residues, is equivalent in both HYP and wild-type mice.[16] The synthesis of apatite is dependent upon the collagen matrix and fibril crosslinking, with nucleation occurring within the 40 nm wide overlapping fibril gaps before proceeding along the long axis of the collagen fibril.[38–40] Thus, the primary influence on the structural changes of apatite in HYP mice is most likely dependent upon phosphate-wasting and not on intrinsic abnormalities of the collagen matrix.

Murine bone hydroxyapatite shares significant similarities to human bone and dentin hydroxyapatite.[14,41] However, the ability to obtain bone tissue from patients with XLH limits the study of mineral apatite in the context of a phosphate-wasting disorder in humans. In addition, during development and as a consequence of bone remodeling and aging, bone composition, including carbonate substitution and crystal maturity varies.[10,34,42–45] In contrast, the use of mature dentin as a model that does not undergo remodeling[46] allows us to capture the composition of a collagenous mineralized matrix in the context of a phosphate-wasting disorder.

Therefore, we employed the use of tooth dentin apatite obtained from individuals with XLH to serve as physiological proxy for bone because it is structurally analogous to bone apatite in several important ways.[9,47] Both apatites display similar crystallite size; both exhibit a relative lack of hydroxylation within the perpendicular channel of the unit cell hexagons; and both display a similar degree of naturally occurring carbonate ion substitution. The use of dentin as a bone equivalent is also validated by the similar particle shape and ordering of the mineral phase within the collagenous matrix in the two tissues at the nanoscale level.[9,48] Because there was little variability in carbonate ion substitution between sexes (control and XLH) data were combined. The small sample size represents a potential limitation of the study and sex differences may become apparent in a larger trial.

Vibrational spectroscopies, such as Raman spectroscopy and FTIR, detect the vibrational modes related to different molecular groups within a material. Band positions and overall band shape are sensitive to changes in nearest neighbor composition and the site symmetry of the molecular group, respectively, allowing these techniques to be used to characterize changing parameters associated with materials, for example, the mineral phase present in bone and teeth. While Raman active modes exhibit a change in the polarizability of the molecular group, FTIR active modes exhibit a change in the dipole moment, implying the commonly observed inverse proportionality between the intensity of FTIR and Raman bands, the reason for which both of these spectroscopic techniques were

employed in this study. Vibrational spectroscopy analysis of tooth dentin indicates a significant increase in carbonate ion substitution in apatite of adult XLH tooth samples, but not in primary teeth, the crowns of which develop *in utero* (Figure 4).[15] This observation is consistent with our previous finding that maternal adaptations occur to meet the mineral demands of pregnancy and lactation in HYP mice.[16] This also aligns with findings that FGF23 does not cross the placental barrier in HYP mice, and that the skeleton of affected offspring is phenotypically indistinguishable from wild-type littermates. Phosphate-wasting ensues shortly after birth, reflective of elevated FGF23 levels and inhibition of renal tubule expression of sodium phosphate symporters.[16,49,50] However, because dental abscesses occur during childhood in primary teeth, these data suggest that mineral defects other than anionic substitution, such as dental pulp necrosis and abnormal mineralization, are contributing factors to pulp infection during childhood.[18,51] In contrast, carbonate ion substitution is significantly increased in permanent tooth dentin of adults with XLH relative to unaffected adults (Figure 4), the postnatal period during which adult tooth development occurs in a phosphate-wasting environment. While we also observed areas of hypomineralization in human XLH dentin[14] by von Kossa staining (data not shown), abscess formation may additionally be potentiated in the adult by carbonate ion substitution and increased dissolution rates, as discussed below, in response to oral acid exposure.

Bone apatite is distinctly different from its geological counterpart, exhibiting a platy or plate-like habit rather than hexagonal, the preferential growth direction dictated by collagen.[48,52,53] Similarly, its size is restricted to the nanometer scale,[48] potentially due to limitations in the maturation of apatite. This produces a material that is more easily resorbable, making it functionally adapted to the process of continual bone remodeling.[54] In addition, the structure of the apatite mineral system, which includes hydroxyapatite, enables it to incorporate a large range of different elements and molecular groups through substitution. At the elemental level, stoichiometric hydroxyapatite $(Ca_{10}(PO_4)_6(OH)_2)$ nanocrystals would be predicted to have a Ca/P molar ratio of 1.67.[55] However, this ratio is lower in bone as the result of cationic substitutions that exceed the anionic substitutions for phosphate. With the inverse proportionality between the Ca/P molar ratio and the solubility of calcium phosphates[56,57] increased resorbability is expected to result from one such stoichiometric change. Conversely, while a number of cations substitute calcium, the most common physiological anionic substitutions in biological hydroxyapatites, including bone and dentin, is anionic, specifically phosphate-to-carbonate, with an estimated occurrence of approximately 2–8 wt.% in healthy bone.[13,58–60] Incorporation of divalent carbonates in place of trivalent phosphates typically creates calcium vacancies in the lattice, which leads to the accumulation of defects and a corresponding decrease of crystallinity and an increase of microstrain,[61] which increases the solubility and makes the material more prone to resorption. In both murine and human samples, the symmetric C-O stretch, ν_1, of the carbonate ion was resolved at 1070 cm^{-1}, indicating B-type substitution of the carbonate ion in bone and dentin. Only minor contributions of the ν_1 (carbonate) band at 1100 cm^{-1} was observed, indicating that A-type substitution is minimal, consistent with other spectroscopic studies of bone and dentin.[9,58]

The functional impact of carbonate substitution for phosphate on the structure of apatite and increased dissolution rates during normal bone remodeling can be considered in the context of differences in charge and atomic radii between the two anions. First, unlike phosphate, carbonate is a planar ion, second, carbonate is significantly smaller than the phosphate ion, as its radius equals 178 pm compared with 238 pm for phosphate. Further, the charge of the carbonate ion is less than that of the phosphate anion necessitating paired substitution to maintain charge neutrality within the crystal structure (Figure 1).[62,63] In addition, recent studies investigated the physiologic response to higher carbonate substitution using synthetic biomaterials with varying amounts of carbonate and revealed that higher carbonate content resulted in increased RANKL secretion and osteoclastogenesis.[11] In light of our data, the structural disorder brought about by additional increases in carbonate ion substitution in XLH would be predicted to further lower the interfacial energy of the material and the barrier for dissolution and growth, with enhanced bone mineral loss.[60] Hence, changing the chemistry of bone mineral materials has important consequences for its stability and the chemical feedbacks occurring within the bone system. Interestingly we found that carbonate ion substitution increased in both wild-type and HYP mice during lactation, the period of

highest skeletal mineral demand in females.[16] It is conceivable that an increased solubility of apatite resulting from its carbonization facilitates further ion release and exchange to satisfy the increased mineral demand of the organism under physiological maternal conditions. The resorption of a carbonate-enhanced apatite may also contribute to the highest reported rates of bone turnover in females, which occurs post-lactation, to restore skeletal mineral to pre-pregnancy levels.[64,65]

In summary, we demonstrate changes in the stoichiometry of mineral in human dentin apatite obtained from individuals with XLH, serving as a proxy for bone. These studies show that, similar to HYP mouse bone, carbonate ion substitution is higher in individuals with XLH. The introduction of additional carbonate into apatite would presumably decrease crystallinity and further increase the level of mineral structural instability, representing an additional challenge in the management of the comorbidities of mineralized tissues associated with phosphate-wasting disorders,[7,16,54,66,67] including the significant number of dental abscesses without caries in the acid environment of the oral cavity.[5,14,18]

The use of adult XLH teeth as a proxy for bone for the study of hydroxyapatite[31] will enable a more comprehensive study of the mineralized matrix in a phosphate-wasting disorder and will also facilitate a better understanding of the forces that regulate the known phenomena of ion substitution in biological apatite. Future studies should focus on determining the degree of molecular adaptation that might occur, including the introduction of ionic vacancies and hydrogen-bonding bridges. Tooth as a bone equivalent will also be useful to determine the impact of increased carbonate substitution on mechanical loading.

Conflict of interest statement

The author(s) declared no potential conflicts of interest with respect to the research, authorship, and/or publication of this article.

References

1. Feng JQ, Clinkenbeard EL, Yuan B, *et al*. Osteocyte regulation of phosphate homeostasis and bone mineralization underlies the pathophysiology of the heritable disorders of rickets and osteomalacia. *Bone* 2013; 54: 213–221.

2. Bielesz B. Emerging role of a phosphatonin in mineral homeostasis and its derangements. European journal of clinical investigation. *Eur J Clin Invest* 2006; 36(Suppl. 2): 34–42.

3. Bowe AE, Finnegan R, Jan de Beur SM, *et al*. FGF-23 inhibits renal tubular phosphate transport and is a PHEX substrate. *Biochem Biophys Res Commun* 2001; 284: 977–981.

4. Wohrle S, Bonny O, Beluch N, *et al*. FGF receptors control vitamin D and phosphate homeostasis by mediating renal FGF-23 signaling and regulating FGF-23 expression in bone. *J Bone Miner Res* 2011; 26: 2486–2497.

5. Carpenter TO, Imel EA, Holm IA, *et al*. A clinician's guide to X-linked hypophosphatemia. *J Bone Miner Res* 2011; 26: 1381–1388.

6. Berndt M, Ehrich JH, Lazovic D, *et al*. Clinical course of hypophosphatemic rickets in 23 adults. *Clin Nephrol* 1996; 45: 33–41.

7. Liang G, Katz LD, Insogna KL, *et al*. Survey of the enthesopathy of X-linked hypophosphatemia and its characterization in Hyp mice. *Calcif Tissue Int* 2009; 85: 235–246.

8. Reid IR, Hardy DC, Murphy WA, *et al*. X-linked hypophosphatemia: a clinical, biochemical, and histopathologic assessment of morbidity in adults. *Medicine* 1989; 68: 336–352.

9. Wopenka B and Pasteris JD. A mineralogical perspective on the apatite in bone. *Mater Sci Eng C* 2005; 25: 131–143.

10. Akkus O, Adar F and Schaffler MB. Age-related changes in physicochemical properties of mineral crystals are related to impaired mechanical function of cortical bone. *Bone* 2004; 34: 443–453.

11. Nakamura M, Hiratai R, Hentunen T, *et al.* Hydroxyapatite with high carbonate substitutions promotes osteoclast resorption through osteocyte-like cells. *ACS Biomater Sci Eng* 2016; 2: 259–267.

12. Rey C, Collins B, Goehl T, *et al.* The carbonate environment in bone mineral: a resolution-enhanced Fourier Transform Infrared Spectroscopy Study. *Calcif Tissue Int* 1989; 45: 157–164.

13. Vallet-Regi M and Navarette DA. *Nanoceramics in clinical use: from materials to applications.* 2nd ed. Cambridge: Royal Society of Chemistry, 2015.

14. Foster BL, Nociti FH Jr and Somerman MJ. The rachitic tooth. *Endocr Rev* 2014; 35: 1–34.

15. Nelson SJ and Ash MM. *Wheeler's dental anatomy, physiology, and occlusion.* 9th ed. St. Louis, MO: Saunders/Elsevier, 2010, xvi, 346 p.

16. Macica CM, King HE, Wang M, *et al.* Novel anatomic adaptation of cortical bone to meet increased mineral demands of reproduction. *Bone* 2016; 85: 59–69.

17. Logan WHG and Kronfeld R. Development of the human jaws and surrounding structures from birth to the age of fifteen years. *J Am Dent Assoc* 1933; 20: 379–427.

18. Linglart A, Biosse-Duplan M, Briot K, *et al.* Therapeutic management of hypophosphatemic rickets from infancy to adulthood. *Endocr Connect* 2014; 3: R13–R30.

19. Camacho NP, Hou L, Toledano TR, *et al.* The material basis for reduced mechanical properties in oim mice bones. *J Bone Miner Res* 1999; 14: 264–272.

20. Gadeleta SJ, Boskey AL, Paschalis E, *et al.* A physical, chemical, and mechanical study of lumbar vertebrae from normal, ovariectomized, and nandrolone decanoate-treated cynomolgus monkeys (Macaca fascicularis). *Bone* 2000; 27: 541–550.

21. Neuman WF and Neuman MW. *The chemical dynamics of bone mineral.* Chicago: The University of Chicago Press, 1958.

22. Boskey A, Frank A, Fujimoto Y, *et al.* The PHEX transgene corrects mineralization defects in 9-month-old hypophosphatemic mice. *Calcif Tissue Int* 2009; 84: 126–137.

23. Camacho NP, Rimnac CM, Meyer RA Jr, *et al.* Effect of abnormal mineralization on the mechanical behavior of X-linked hypophosphatemic mice femora. *Bone* 1995; 17: 271–278.

24. Coyac BR, Hoac B, Chafey P, *et al.* Defective mineralization in X-linked hypophosphatemia dental pulp cell cultures. *J Dent Res* 2018; 97: 184–191.

25. Awonusi A, Morris MD and Tecklenburg MM. Carbonate assignment and calibration in the Raman spectrum of apatite. *Calcif Tissue Int* 2007; 81: 46–52.

26. Biltz RM and Pellegrino ED. The nature of bone carbonate. *Clin Orthop Relat Res* 1977; 129: 279–292.

27. Pellegrino ED, Biltz RM and Letteri JM. Inter-relationships of carbonate, phosphate, monohydrogen phosphate, calcium, magnesium and sodium in uraemic bone: comparison of dialysed and non-dialysed patients. *Clin Sci Mol Med* 1977; 53: 307–316.

28. Wentrup-Byrne E, Armstrong CA, Armstrong RS, *et al.* Fourier transform Raman microscopic mapping of the molecular components in a human tooth. *J Raman Spectros* 1997; 28: 151–158.

29. Frushour BG and Koenig JL. Raman scattering of collagen, gelatin, and elastin. *Biopolymers* 1975; 14: 379–391.

30. Penel G, Leroy G, Rey C, *et al.* MicroRaman spectral study of the PO4 and CO3 vibrational modes in synthetic and biological apatites. *Calcif Tissue Int* 1998; 63: 475–481.

31. Opsahl Vital S, Gaucher C, Bardet C, *et al.* Tooth dentin defects reflect genetic disorders affecting bone mineralization. *Bone* 2012; 50: 989–997.

32. Balan E, Delattre S, Roche D, *et al.* Line-broadening effects in the powder infrared spectrum of apatite. *Phys Chem Miner* 2011; 38: 111–122.

33. Farlay D, Panczer G, Rey C, *et al.* Mineral maturity and crystallinity index are distinct characteristics of bone mineral. *J Bone Miner Metab* 2010; 28: 433–445.

34. Paschalis EP, DiCarlo E, Betts F, *et al.* FTIR microspectroscopic analysis of human osteonal bone. *Calcif Tissue Int* 1996; 59: 480–487.

35. Poralan GM Jr, Gambe JE, Alcantara EM, *et al.* X-ray diffraction and infrared spectroscopy analyses on the crystallinity of engineered biological hydroxyapatite for medical application. *IOP Conf Ser Mater Sci Eng* 2015; 79: 012028.

36. Dey A, Bomans PH, Muller FA, *et al*. The role of prenucleation clusters in surface-induced calcium phosphate crystallization. *Nat Mater* 2010; 9: 1010–1014.

37. Rai DV, Darbari R and Aggarwal LM. Age-related changes in the elemental constituents and molecular behaviour of bone. *Indian J Biochem Biophys* 2005; 42: 127–130.

38. Glimcher MJ. The nature of the mineral component of bone and the mechanism of calcification. *Instr Course Lect* 1987; 36: 49–69.

39. Landis WJ, Song MJ, Leith A, *et al*. Mineral and organic matrix interaction in normally calcifying tendon visualized in three dimensions by high-voltage electron microscopic tomography and graphic image reconstruction. *J Struct Biol* 1993; 110: 39–54.

40. Moradian-Oldak J, Weiner S, Addadi L, *et al*. Electron imaging and diffraction study of individual crystals of bone, mineralized tendon and synthetic carbonate apatite. *Connect Tissue Res* 1991; 25: 219–228.

41. Weijs WA and Dantuma R. Electromyography and mechanics of mastication in the albino rat. *J Morphol* 1975; 146: 1–33.

42. Boskey AL and Coleman R. Aging and bone. *J Dent Res* 2010; 89: 1333–1348.

43. Verdelis K, Lukashova L, Wright JT, *et al*. Maturational changes in dentin mineral properties. *Bone* 2007; 40: 1399–1407.

44. Verdelis K, Lukashova L, Yamauchi M, *et al*. Changes in matrix phosphorylation during bovine dentin development. *Eur J Oral Sci* 2007; 115: 296–302.

45. Handschin RG and Stern WB. Crystallographic lattice refinement of human bone. *Calcif Tissue Int* 1992; 51: 111–120.

46. Boskey A. Mineralization of bones and teeth. *Elements* 2007; 3: 387–393.

47. Pasteris JD, Wopenka B, Freeman JJ, *et al*. Lack of OH in nanocrystalline apatite as a function of degree of atomic order: implications for bone and biomaterials. *Biomaterials* 2004; 25: 229–238.

48. Bocciarelli DS. Morphology of crystallites in bone. *Calcif Tissue Res* 1970; 5: 261–269.

49. Kovacs CS. Calcium and bone metabolism disorders during pregnancy and lactation. *Endocrinol Metab Clin North Am* 2011; 40: 795–826.

50. Ma Y, Kirby BJ, Fairbridge NA, *et al*. FGF23 is not required to regulate fetal phosphorus metabolism but exerts effects within 12 hours after birth. *Endocrinology* 2017; 158: 252–263.

51. Chaussain-Miller C, Sinding C, Septier D, *et al*. Dentin structure in familial hypophosphatemic rickets: benefits of vitamin D and phosphate treatment. *Oral Dis* 2007; 13:482–489.

52. Glimcher MJ, Hodge AJ and Schmitt FO. Macromolecular aggregation states in relation to mineralization: the collagen-hydroxyapatite system as studied in vitro. *Proc Natl Acad Sci U S A* 1957; 43: 860–867.

53. Bocciarelli DS. Apatite microcrystals in bone and dentin. *J Microsc* 1973; 16: 21–34.

54. Skinner HCW. Mineralogy of bones. In: Selinus O (ed.) *Essentials of medical geology: revised edition*. Dordrecht: Springer Netherlands, 2013, pp.665–687.

55. LeGeros RZ and Legeros JP. Phosphate minerals in human tissues. In: Nriagu JO and Moore PB (eds) *Phosphate minerals*. Berlin, Heidelberg: Springer Berlin Heidelberg, 1984, pp.351–385.

56. Chow LC. Solubility of calcium phosphates. *Monogr Oral Sci* 2001; 18: 94–111.

57. Uskokovic V and Desai TA. Phase composition control of calcium phosphate nanoparticles for tunable drug delivery kinetics and treatment of osteomyelitis. I. Preparation and drug release. *J Biomed Mater Res A* 2013; 101: 1416–1426.

58. LeGeros RZ. Calcium phosphates in oral biology and medicine. *Monogr Oral Sci* 1991; 15: 1–201.

59. Nanci A, Wazen R, Nishio C, *et al*. Immunocytochemistry of matrix proteins in calcified tissues: functional biochemistry on section. *Eur J Histochem* 2008; 52: 201–214.

60. Nelson DG, Featherstone JD, Duncan JF, *et al*. Paracrystalline disorder of biological and synthetic carbonate-substituted apatites. *J Dent Res* 1982; 61: 1274–1281.

61. Baig AA, Fox JL, Young RA, *et al*. Relationships among carbonated apatite solubility, crystallite size, and microstrain parameters. *Calcif Tissue Int* 1999; 64: 437–449.

62. Peroos S, Du Z and de Leeuw NH. A computer modelling study of the uptake, structure and distribution of carbonate defects in hydroxy-apatite. *Biomaterials* 2006; 27: 2150–2161.

63. Pan Y and Fleet ME. Compositions of the apatite-group minerals: substitution mechanisms and controlling factors. *Rev Mineral Geochem* 2002; 48: 13–49.

64. Bowman BM and Miller SC. Skeletal mass, chemistry, and growth during and after multiple reproductive cycles in the rat. *Bone* 1999; 25: 553–559.

65. Miller SC and Bowman BM. Rapid improvements in cortical bone dynamics and structure after lactation in established breeder rats. *Anat Rec A Discov Mol Cell Evol Biol* 2004; 276: 143–149.

66. Karaplis AC, Bai X, Falet JP, *et al*. Mineralizing enthesopathy is a common feature of renal phosphate-wasting disorders attributed to FGF23 and is exacerbated by standard therapy in hyp mice. *Endocrinology* 2012; 153: 5906–5917.

67. Liang G, Vanhouten J and Macica CM. An atypical degenerative osteoarthropathy in Hyp mice is characterized by a loss in the mineralized zone of articular cartilage. *Calcif Tissue Int* 2011; 89: 151–162.

Visit SAGE journals online
journals.sagepub.com/home/taj

§SAGE journals